Nonmuscle myosin II powered transport of newly formed collagen fibrils at the plasma membrane

Nicholas S. Kalson[a,1], Tobias Starborg[a,1], Yinhui Lu[a], Aleksandr Mironov[b], Sally M. Humphries[a], David F. Holmes[a], and Karl E. Kadler[a,2]

[a]Wellcome Trust Centre for Cell-Matrix Research and [b]Faculty of Life Sciences, University of Manchester, Manchester M13 9PT, United Kingdom

Edited by Darwin J. Prockop, Texas A&M Health Science Center, Temple, TX, and approved October 15, 2013 (received for review July 30, 2013)

Collagen fibrils can exceed thousands of microns in length and are therefore the longest, largest, and most size-pleomorphic protein polymers in vertebrates; thus, knowing how cells transport collagen fibrils is essential for a more complete understanding of protein transport and its role in tissue morphogenesis. Here, we identified newly formed collagen fibrils being transported at the surface of embryonic tendon cells in vivo by using serial block face-scanning electron microscopy of the cell-matrix interface. Newly formed fibrils ranged in length from ∼1 to ∼30 μm. The shortest (1–10 μm) occurred in intracellular fibricarriers; the longest (∼30 μm) occurred in plasma membrane fibripositors. Fibrils and fibripositors were reduced in numbers when collagen secretion was blocked. ImmunoEM showed the absence of lysosomal-associated membrane protein 2 on fibricarriers and fibripositors and there was no effect of leupeptin on fibricarrier or fibripositor number and size, suggesting that fibricarriers and fibripositors are not part of a fibril degradation pathway. Blebbistatin decreased fibricarrier number and increased fibripositor length; thus, nonmuscle myosin II (NMII) powers the transport of these compartments. Inhibition of dynamin-dependent endocytosis with dynasore blocked fibricarrier formation and caused accumulation of fibrils in fibripositors. Data from fluid-phase HRP electron tomography showed that fibricarriers could originate at the plasma membrane. We propose that NMII-powered transport of newly formed collagen fibrils at the plasma membrane is fundamental to the development of collagen fibril-rich tissues. A NMII-dependent cell-force model is presented as the basis for the creation and dynamics of fibripositor structures.

3View | SBF-SEM | extracellular matrix | vesicle | actin

Cells have sophisticated mechanisms for transporting proteins from one location to another, often within membrane-bound vesicles that need to be of appropriate size and shape to accommodate the cargo. Collagen is a special case and is used as a model protein for studying protein transport; not only is collagen the most abundant structural protein in vertebrates, but it is too large to be accommodated within conventional transport vesicles. Moreover, collagen molecules self-assemble into structures of increasing size with each successive stage in the secretory pathway. The transported cargo increases from ∼0.5 MDa in the endoplasmic reticulum (ER) to several teradaltons (TDa) at the plasma membrane where the molecules are organized into fibrils. The motivation for our study was to build a temporal, spatial, and directional road map of the movement of membrane-bound collagen fibrils at the plasma membrane as the basis for a complete understanding of how cells transport collagen in the process of assembling a mechanically functional extracellular matrix (ECM).

In brief, procollagen (the biosynthetic precursor of collagen) is synthesized in the ER and is asymmetric and relatively large; triple helical procollagen molecules are ∼1.5 nm diameter, ∼300 nm long, and have mass of ∼450 kDa. Tubular-saccular carriers containing procollagen arise from specialized ER domains (1, 2). TANGO1 recruits Sedlin and steers procollagen into COPII-dependent ER exit sites (3, 4) before CUL3-KLHL12 ubiquitinates a pool of sec31 molecules to drive procollagen transport from the ER to the Golgi apparatus (reviewed by ref. 5). ER-to-Golgi carriers join the Golgi stacks by fusing with *cis* cisternae and induce the formation of intercisternal tubules. Procollagen traverses the Golgi apparatus without leaving the cisternal lumen (6, 7). Once through the Golgi apparatus, procollagen can travel in pleomorphic Golgi-to-plasma membrane carriers (GPCs) that can be 0.3–1.7 μm in length (8). Evidence from electron microscopy suggests that these carriers contain sheaves of procollagen molecules stacked in zero register (9). Conversion of procollagen to collagen culminates in the formation of elongated fibrils that can be millimeters in length and are the primary tensile element of diverse tissues (10–12). Different types of collagen polymerize and form complexes with proteoglycans and other glycoproteins to form the largest assembles in vertebrate tissues (reviewed by ref. 13). The fibrils are deposited in embryonic tissues where they are ∼30 nm in diameter and contain ∼350 collagen molecules in the cross-section (based on calculations by ref. 14); thus, the fibrils are ∼0.3 TDa/μm. Considering that the first-formed fibrils are a few microns in length and grow to several millimeters, the fibrils are the largest size range structures transported by cells.

The fact that collagen fibrils in vivo are too narrow and too densely packed to be resolved by light microscopy precludes real-time studies of cell–fibril interactions in vivo. Thus, transmission electron microscopy (TEM) has emerged as the method of choice for in vivo fibril studies but is not without its challenges because of the tortuosity and extreme lengths of the fibrils. Trelstad and Hayashi, and later Birk and Trelstad, used serial section transmission electron microscopy (ssTEM) to image the cell-matrix

Significance

Collagen is the most abundant protein in vertebrates and is the building block of strong tissues such as tendons, skin, and bones. The fibrils can be millimeters long and occur in the extracellular matrix as a scaffold for tissue growth. Important questions remain unanswered about how cells assemble and transport the fibrils. We show here that collagen fibril assembly can occur at the plasma membrane in structures called fibripositors. We show that fibripositors are a nonmuscle myosin II (NMII)-dependent mechanical interface between the actinomyosin machinery and the extracellular matrix; thus, we propose a new function for NMII. A unique mechanism of fibril transport is presented as a basis for studies of tissue morphogenesis and conditions including wound healing and fibrosis.

Author contributions: N.S.K., T.S., and K.E.K. designed research; N.S.K., T.S., Y.L., A.M., and S.M.H. performed research; N.S.K., T.S., D.F.H., and K.E.K. analyzed data; and N.S.K., D.F.H., and K.E.K. wrote the paper.

The authors declare no conflict of interest.

This article is a PNAS Direct Submission.

Freely available online through the PNAS open access option.

[1]N.S.K. and T.S. contributed equally to this work.

[2]To whom correspondence should be addressed. E-mail: karl.kadler@manchester.ac.uk.

This article contains supporting information online at www.pnas.org/lookup/suppl/doi:10.1073/pnas.1314348110/-/DCSupplemental.

interface in embryonic tendon and were among the first to identify collagen fibrils in plasma membrane recesses (15, 16). Using data from an image stack of ∼14 μm depth (which is approximately one-fourth the length of an embryonic tendon cell; ref. 15), Trelstad and Hayashi proposed that the fibrils are formed by the addition of subassemblies of collagen onto the ends of the fibrils in plasma membrane recesses (15). In later studies, using image stacks of depth ∼20 μm, Canty and coworkers described actin-dependent slender projections (called fibripositors) that contained deeper recesses in which collagen fibrils were located (17, 18). The number of sections that can be cut for ssTEM limits the practicality of viewing entire cells and complete fibrils. However, serial block face-scanning electron microscopy (SBF-SEM; ref. 19) has emerged as a practical alternative to ssTEM for studying collagen fibril assembly in vivo (20).

The experiments described below used SBF-SEM to study how cells transport collagen fibrils in vivo. We identified an abundance of short newly formed fibrils associated with a variety of plasma membrane morphologies and within intracellular fibricarriers; fibricarriers were identified that were larger than the GPCs and fibril vesicles that have been described previously. We show that collagen fibrils in fibricarriers and fibripositors decrease in abundance when procollagen secretion from the ER is blocked by dimethyloxaloylglycine (DMOG), which is a potent inhibitor of prolyl 4-hydroxylase (21). We show that fibricarriers can originate at the plasma membrane and are transported into fibricarriers powered by nonmuscle myosin II (NMII) in a process that is blocked by dynasore inhibition of dynamin-dependent endocytosis (22). We propose a unique transport pathway in which new collagen fibrils assembling on the cell surface are moved through the cell in a process powered by NMII.

Results

Visualization of Entire Collagen Fibrils in Fibripositors and Fibricarriers. Fourteen-day-old chicken embryonic tendon was prepared for SBF-SEM by using 3View as described (20), and image analysis was performed by using IMOD (23). Fig. 1*A* shows a 3D reconstruction of a typical cell that is elongated along the long axis of the tendon and is surrounded by an ECM containing densely packed 30-nm-diameter collagen fibrils (Fig. 1*B*). The z range used in the experiment was sufficient to track complete collagen fibrils at the cell-matrix interface in plasma membrane recesses (Fig. 1*C*).

Fig. 2 *A* and *B* show data from two further cells. Examples of fibrils with one tip in the ECM (the distal tip) and the other tip in fibripositors (the proximal tip) are highlighted blue and green. Approximately two-thirds of the number of fibripositors observed had a finger-like protrusion of the plasma membrane. We called these structures "protruding fibripositors." The remainder of the fibripositors had the characteristic slender invagination of the plasma membrane without the finger-like protrusion. We called these "recessed fibripositors." The fibril highlighted in

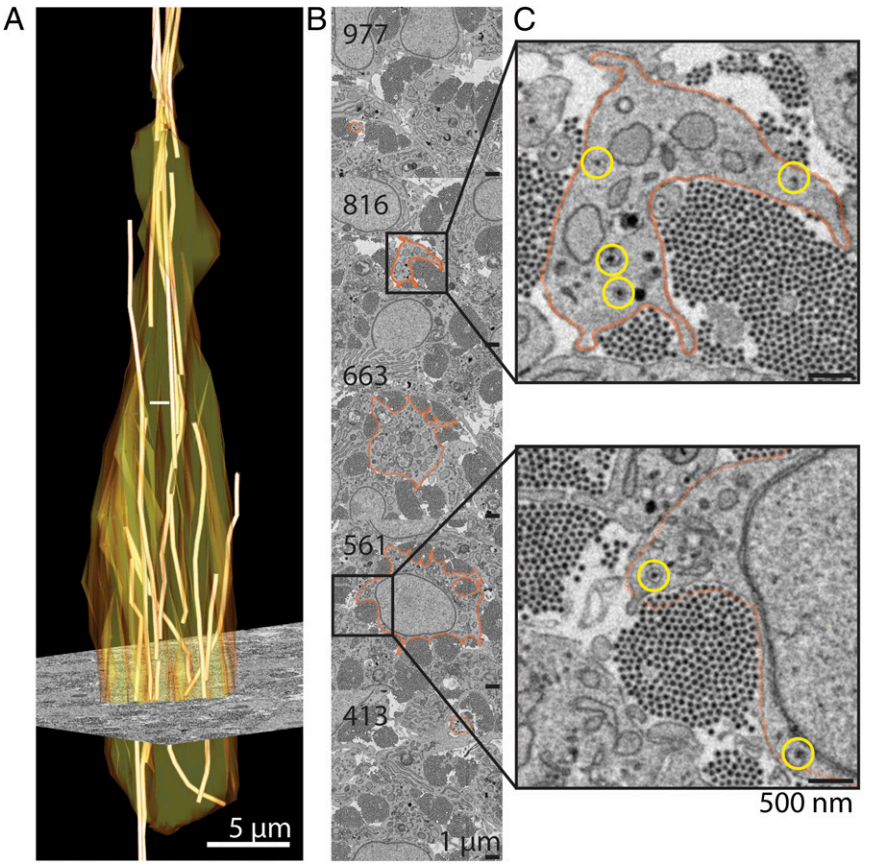

Fig. 1. Visualization of entire collagen fibrils at the cell-matrix interface by 3View SBF-SEM. SBF-SEM analysis of 14-d embryonic chick tendon with dimensions 30 μm × 30 μm × 100 μm (*x*, *y*, and *z*, respectively, with the *z* axis parallel to the long axis of the tendon) achieved by making 1,000 × 100 nm-thick cuts. The images were used for image analysis in IMOD. (*A*) Three-dimensional reconstruction of a single cell (outlined in orange) showing collagen fibrils (yellow) closely associated with the plasma membrane. An EM image is shown superimposed on the reconstruction. (*B*) Selected areas from cuts 413, 561, 663, 816, and 977. Orange, the plasma membrane of the cell. (*C*) Higher magnification views of cuts 561 and 816. Orange, the plasma membrane of the cell; yellow circles, collagen fibrils in cytoplasmic compartments.

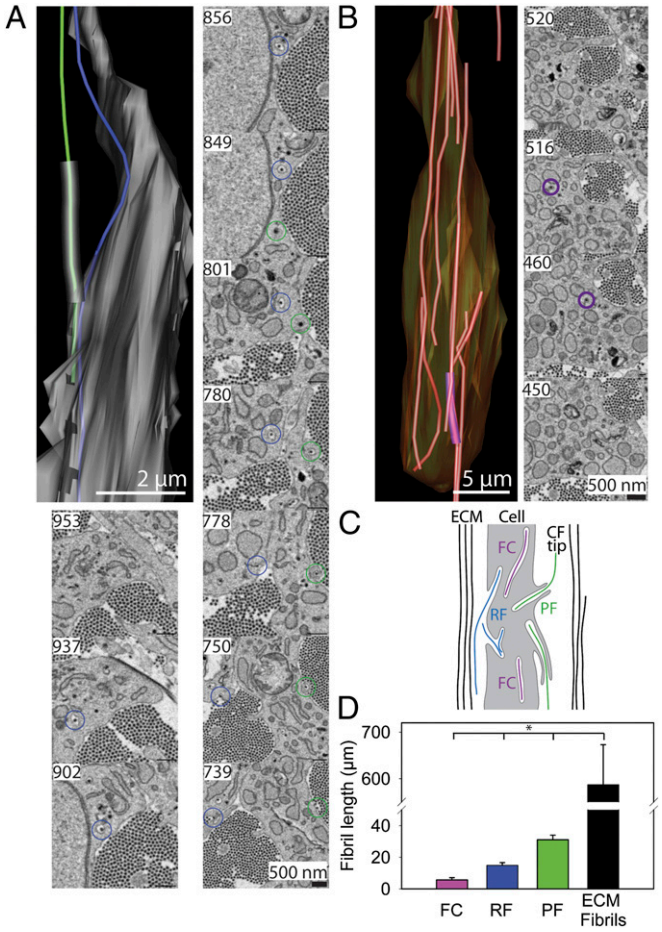

Fig. 2. Quantitative length measurements of collagen fibrils in vivo. SBF-SEM volume of 14-d embryonic chick tendon with dimensions 30 μm × 30 μm × 100 μm (*x*, *y*, and *z*, respectively) achieved by making 1,000 × 100 nm-thick cuts. The images were used for image analysis in IMOD. (*A*) Part of a 3D reconstruction of a cell between cuts 739 and 953, equivalent to 21.4 μm along the long axis of the cell. EM images show selected areas of the cell-matrix interface. A collagen fibril (green) is shown with one tip at the base of the plasma membrane recess and the other extending through a protruding fibripositor with the other tip in the ECM (green line in the reconstruction and green circle in the 3View images). Also shown is a collagen fibril with a tip within a plasma membrane recess and exiting the cell through a recessed fibripositor (blue). This dataset is shown in Movie S1. (*B*) Three-dimensional reconstruction of another cell showing a collagen fibril entirely contained within a membrane-bound cytoplasmic fibricarrier (purple). Selected cuts containing the fibricarrier are also shown with the fibricarrier circled in purple (520, 516, 460, and 450). This dataset in shown in Movie S2. (*C*) Schematic representation of the cell-matrix interface, illustrating the three membrane-fibril structures identified (FC, fibricarriers; PF, protruding fibripositors; RF, recessed fibripositors). Color scheme remains the same as in *A* and *B*. (*D*) Quantitation of the lengths of fibrils in fibricarriers, recessed fibripositors, protruding fibripositors, and in the ECM. *, significant difference in fibril length ($P \leq 0.05$).

green (Fig. 2*A*) is representative of a fibril with its proximal tip within a protruding fibripositor and its distal tip in the ECM. The fibril highlighted in blue has its distal tip in the ECM and its proximal tip within a recessed fibripositor (shown schematically in Fig. 2*C*). Movie S1 is a movie showing a recessed fibripositor and a protruding fibripositor. Fig. 2*B* shows a collagen fibril enclosed within a fibricarrier. Fibricarriers accounted for ∼5% of fibril-containing compartments (i.e., fibricarriers + recessed fibripositors + protruding fibripositors). The fibril in the fibricarrier is highlighted purple in the 3D reconstruction and 3View images. The 3View images of a fibricarrier are shown in Movie S2. The lengths of fibrils in the different compartments were as follows: fibricarriers (5.7 ± 1.4 μm), recessed fibripositors (14.9 ± 1.7 μm), and protruding fibripositors (31.2 ± 2.9 μm; Fig. 2*D*). Fibrils leaving the cell through recessed fibripositors were commonly seen to run along the external surface of the cell before either terminating in a fibril tip or tracking away from the cell surface and entering a bundle of fibrils. Conversely, fibrils leaving the cell in protruding fibripositors were positioned with the end of the membrane protrusion within a fibril bundle. This difference in fibril positioning is demonstrated in Fig. 2*A* in which the recessed fibripositor fibril runs along the surface of the cell (blue fibril), whereas the protruding fibripositor projects directly into the matrix (green fibril). The length of the finger-like component of protruding fibripositors ranged from <1–25.7 μm. It is noteworthy that even at this early stage of development [embryonic day (E) 14 in the chick], some fibrils in the ECM were too long to be enclosed in a typical 100-μm z-depth volume. Therefore, a length estimate was made by using the method described (20). The estimated matrix fibril length was 587 ± 86 μm and, therefore, much longer than those found in either recessed or protruding fibripositors.

No Evidence of Collagen Fibril Degradation in Fibricarriers. Intracellular vacuoles containing collagen fibrils have been described in periodontal ligament, some of which contain a densely stained material between the fibril and the vacuole membrane (24–27). Blocking lysosomal enzymes in periodontal ligament resulted in accumulation of intracellular vacuolar fibrils (28, 29), suggesting that collagen fibrils could be degraded in lysosomal compartments.

To explore the possibly that fibricarriers could be part of a fibril degradation pathway, we first carefully examined the ultramicroscopic appearance of fibricarriers. Electron-dense fibricarriers were not observed in embryonic tendon; all fibricarriers were electron lucent. Furthermore, fibricarriers containing degraded fibril aggregates were absent. The absence of these morphological structures reduces the likelihood that fibrils in fibricarriers are degraded. To explore this hypothesis further, we performed immunoEM on E15.5 mouse-tail tendon for lysosomal-associated membrane protein 2 (LAMP2), a marker of lysosomes and late endosomes (30). As shown in Fig. 3*A*, LAMP2 is abundant in multivesicular compartments typical of late endosomes but absent from fibripositors and fibricarriers. Next, we incubated living tendon with leupeptin and used SBF-SEM to quantitate the occurrence of fibricarriers. To test the efficacy of leupeptin to inhibit lysosomal proteases, control experiments were carried out in which we incubated tendon fibroblasts with fluorescently labeled epidermal growth factor (EGF) in the presence and absence of leupeptin, using methods described (31). EGF was readily taken up by fibroblasts (Fig. 3*B, Top*). In control cells, after 60-min incubation, the EGF was degraded, with no fluorescently labeled EGF visible (Fig. 3*B, Middle*). In contrast, no EGF degradation occurred in the presence of leupeptin (remaining fluorescent labeled EGF in Fig. 3*B, Bottom*). Having demonstrated the efficacy of leupeptin in tendon fibroblasts, we incubated embryonic tendon in leupeptin. If fibricarriers were part of a lysosomal degradation pathway, treatment with leupeptin would be expected to increase their numbers. However, we found no significant effect of prolonged leupeptin treatment (48 h) on the frequency of fibricarriers or of fibripositors (Fig. 3*C*).

Fibripositors Contain Newly Formed Collagen Fibrils. Tracking of fibrils closely associated with the cell membrane revealed that complete, short-length collagen fibrils occurred on the surface of cells and in fibripositors (Fig. S1 and Movie S3). Furthermore, fibripositor structures contain shorter fibrils than those in the

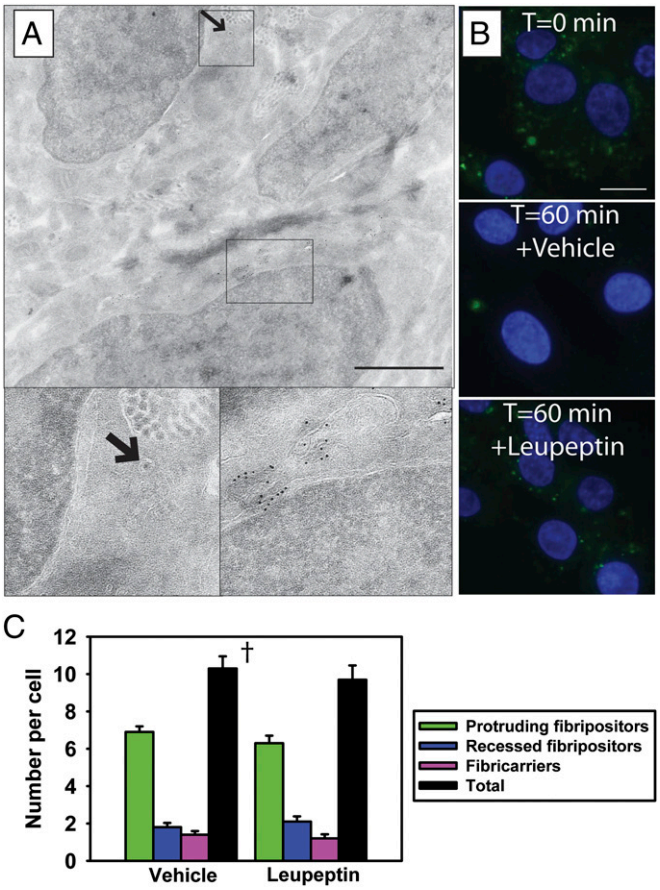

Fig. 3. Cytoplasmic fibrils are not degraded by lysosomal proteases. (*A*) ImmunoEM on cryosections of embryonic mouse tail by using an anti-LAMP2 antibody localized LAMP2 to endosome structures in the cytoplasm but not to collagen fibril-containing compartments (arrow). (*B*) Endocytic uptake of fluorescent-labeled EGFR after 30-min incubation revealed loss of fluorescence in the presence, but not the absence, of leupeptin. (*C*) Quantitation of fibril-containing compartments after treatment with leupeptin. Treatment with leupeptin (48 h) did not affect the proportion of fibrils in recessed or protruding fibripositors or the total number of intracellular fibrils. $^{\dagger}P > 0.05$. (Scale bars: *A*, 1 μm; *B*, 5 μm.)

ECM. These data suggested that fibripositors might be a site of fibril assembly. Therefore, in the next experiment, we incubated tendons with the prolyl 4-hydroxylase inhibitor DMOG (21) for 48 h to block collagen export from the ER (Fig. 4*A*) and examined the cells in situ by SBF-SEM (Fig. 4*B*). The results showed that DMOG reduced the number of short fibrils and fibril-containing compartments (fibricarriers and fibripositors). In particular, the number of protruding fibripositors was reduced from ∼6 per cell in DMSO control samples to ∼1 per cell in DMOG-treated samples (Fig. 4 *B* and *C*). Thus, blocking collagen secretion reduced the number of fibripositors.

Next, we incubated tendons with GM6001 (a broad-spectrum inhibitor of matrix metalloproteinases; MMPs) and used SBF-SEM to identify short fibrils. In contrast to results with DMOG, GM6001 did not prevent the occurrence of short fibrils at the cell surface in fibripositors (representative cell reconstruction in Fig. S2*A*). Zymography showed that GM6001 was active under the conditions used (Fig. S2*B*).

Fibricarriers Can Be Formed at the Plasma Membrane. We used solution-phase horseradish peroxidase (HRP) according to the schematic shown in Fig. 5*A* to investigate if fibricarriers can be formed at the plasma membrane in a process analogous to endocytosis. We subsequently stained with diaminobenzidine (DAB) and osmium, embedded the samples for TEM, performed electron tomography on 63 300-nm–thick serial sections, and stacked the tomograms (Fig. 5 *B–D*) to generate a combined 3D volume of *z* depth 18.9 μm. Examination of the stacked tomogram showed the presence of both electron dense (HRP containing) and electron lucent (not containing HRP) fibricarriers: 15 of 25 fibricarriers were electron dense, whereas 10 were electron lucent.

NMII Powers the Transport of Newly Formed Fibrils at Fibripositors. Meshel et al. showed that cultured fibroblasts use NMII to power the contraction of lamellipodia attached to collagen fibrils, thereby causing the cell to move (32). To test the hypothesis that NMII might power the pulling on fibrils at fibripositors, we used blebbistatin in a 3D tendon-like cell-culture system that successfully recapitulates key aspects of embryonic tendon development (33, 34). We show here that when tension is released in the tendon-like constructs by removal of an anchor post, the constructs contract to approximately one-fifth of their original length (compare Fig. 6*A, Left* and *Center*). However, when the constructs are incubated with blebbistatin no contraction occurred (compare Fig. 6*A, Left* and *Right*). Experiments with embryonic tendon cells in 2D demonstrated that inhibition of NMII resulted in disruption of normal membrane dynamics, with more protrusive activity resulting in longer filopodia, as reported (35) (Fig. 6*B*). SBF-SEM analysis of tendon-like constructs treated with blebbistatin more than doubled the length of the protrusive part of the fibripositor (Fig. 6*C*) and reduced numbers of protruding fibripositors and fibricarriers (Fig. 6 *D* and *E*). Three-dimensional reconstructions are shown in Fig. 6*E*. A schematic representation of the effect of NMII inhibition—fewer, longer protrusive fibripositors, and fewer fibricarriers—is shown in Fig. 6*F*.

In further experiments, we showed that inhibiting dynamin with dynasore resulted in marked disorganization of fibricarriers and fibripositors (Fig. 7). In control samples, single fibrils are seen within the internal part of protrusive fibripositors and in recessed fibripositors (Fig. 7*A, Upper*), whereas in dynasore-treated tendon, multiple fibrils are seen in these compartments (Fig. 7*A, Lower*). Three-dimensional reconstruction revealed that these compartments were morphologically abnormal and disorganized, some looping inside the cell (Fig. 7*B* and Movie S4). Quantification revealed that the length of the protrusive part of fibripositors was not affected by treatment with dynasore (Fig. 7*C*). However, the length of the internal part of protrusive fibripositors and of recessed fibripositors was significantly increased (Fig. 7*D*). Furthermore, similar to the finding in blebbistatin-treated tendon, dynasore reduced the number of fibricarriers (Fig. 7*E*). The finding of long, looped plasma membrane recesses and the absence of fibricarriers (shown schematically in Fig. 7*F*) suggested that internalization of collagen fibrils within fibricarriers (powered by NMII) is an endocytic-like process.

Actin Clustering at Collagen Fibril Interaction Sites in Fibripositors. Previous observations that fibripositors are disassembled after treatment with cytochalasin B (18) prompted analysis of our new datasets for evidence of fibrils being grasped within fibripositors. Longitudinal sections of fibripositors showed the presence of corrugations of the lumen in which the fibril is pinched at ∼10 locations along the length of the fibripositor (Fig. 8*A*). TEM analysis identified increased abundance of intracellular fine filaments, consistent with F-actin, at pinch points (Fig. 8*C*). Three-dimensional reconstructions showed that the pinch points occurred at regular intervals along recessed and protruding fibripositors (Fig. 8*D* and Movie S5).

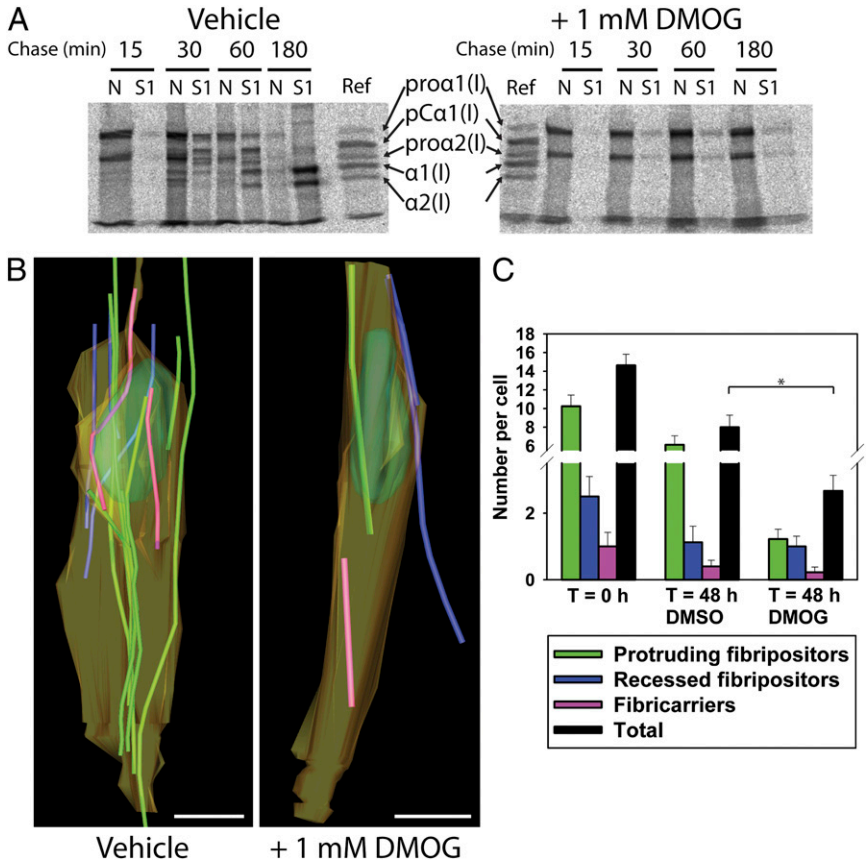

Fig. 4. Protruding and recessed fibripositors contain newly synthesized collagen fibrils. Pulse–chase analysis of embryonic tendon demonstrated that procollagen processing and secretion was prevented by DMOG and reduced the numbers of fibripositors and fibricarriers. (*A*) Proteins were sequentially extracted in neutral salt buffer (S1) and buffer containing Nonidet P-40 (N), and the ^{14}C-labeled proteins were analyzed by SDS/PAGE and autoradiography. The identity of polypeptide chains of procollagen, pC-collagen, and collagen are indicated. (*B*) Visualization of the cell-matrix interface by SBF-SEM before and after treatment with DMOG for 48 h. Fewer fibrils occurred in fibricarriers (purple), protruding (green), and recessed (blue) fibripositors. (Scale bar: 2 μm.) (*C*) Quantitation of the frequency of fibril-containing compartments before and after inhibition of procollagen secretion by DMOG. *$P \leq 0.05$.

Discussion

We have determined the shape, size, and 3D organization of fibripositors and fibricarriers, which contain new collagen fibrils, at the plasma membrane and in the cytoplasm in vivo. It is possible to obtain a spatial map of the origin, location, and size of these compartments that contain fibrils of particular length ranges: Fibrils increased in length in the order of fibricarriers (1–10 μm), recessed fibripositors (5–30 μm), and protruding fibripositors (5–40 μm), with the longest occurring in the ECM (100–600 μm). The steady increase in fibril length suggested that these compartments are part of a common fibril-transport pathway. The inhibition of procollagen synthesis, NMII, and dynamin in conjunction with SBF-SEM 3D reconstruction (20) has indicated the direction of fibril transport.

At first sight, the range of fibril lengths in the different compartments could be interpreted to fit either a degradation or assembly pathway. If degradation is occurring, it could be reasoned that ECM fibrils are progressively reduced in length until the shortest fibrils are contained within fibricarriers. Conversely, fibrils in fibricarriers could grow to become fibrils in recessed fibripositors, then protruding fibripositors, and then released to the ECM. To distinguish between these two possibilities, we used leupeptin to inhibit lysosomal degradation, immunoEM to locate the endosomal marker LAMP2, and DMOG to inhibit procollagen secretion. Studies of periodontal ligament in postnatal mice showed that inhibiting lysosomal function using leupeptin resulted in an increase in vacuolar fibrils (29). Further studies showed that blocking collagen synthesis or disrupting microtubule polymerization (which inhibits collagen secretion; ref. 18) had no effect on the numbers of fibril-containing vacuoles (28). The conclusion from these studies was that collagen fibrils could be segregated from the matrix and degraded within lysosomal compartments. The results here showed that fibricarriers and fibripositors lack LAMP2 staining and are unaffected by leupeptin. Furthermore, their numbers decrease and there is an absence of short fibrils at the plasma membrane in the presence of DMOG. Thus, in the absence of procollagen molecules passing through the secretory pathway, no new fibrils assembled at the cell surface and the number of fibripositors was reduced. We also considered the possibility that short fibrils at the cell surface could be formed by cleavage of preexisting fibrils. Experiments with an MMP inhibitor suggested that active MMPs capable of cleaving collagen molecules are not required for the formation of short fibrils. These experiments showed that fibricarriers and fibripositors contain new collagen fibrils and that the fibrils are not being degraded.

To test if fibricarriers could be formed by internalization of collagen fibrils, we incubated tendon tissue with solution phase HRP. After incubation, a significant proportion of fibricarriers contained a dark precipitate, suggesting that they formed through an endocytic process. It is possible that HRP could be delivered to fibricarriers by pinocytosis of HRP-containing fluid from the ECM and subsequent fusion of the vesicle with fibricarriers. However, the surfaces of fibricarriers were smooth and lacked evidence of overt fusion with other compartments. Non-HRP–stained

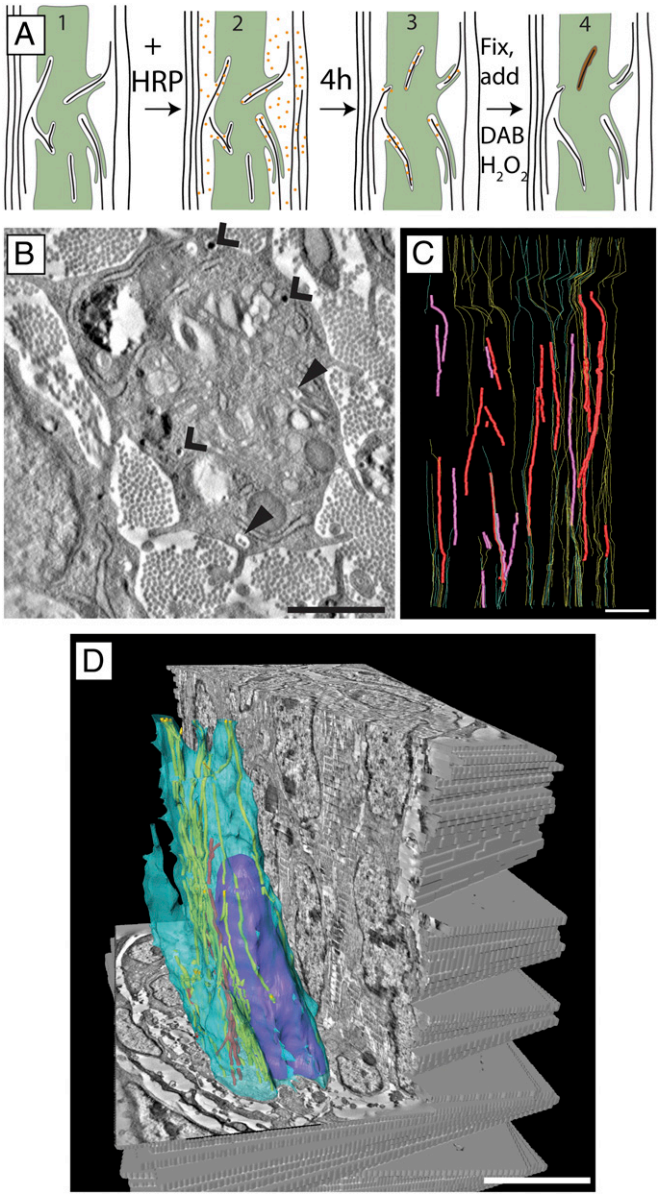

Fig. 5. Fibricarriers can be generated by out-to-in fibril transport. (*A*) Schematic representation of the HRP experiment. Orange dots represent HRP molecules. Brown-colored compartments represent compartments that are positive for electron-dense stain. (*B*) A virtual slice through a 3D EM tomogram of 13-d chicken embryonic metatarsal tendon that had been incubated with HRP solution for 4 h before fixation. Internal fibrils containing an electron-dense precipitate are seen (open arrowhead) together with internal fibrils with no precipitate (closed arrowhead). (*C*) Three-dimensional reconstruction from 65 serial section tomograms. Fibricarriers containing electron dense precipitate are shown in red, fibricarriers with no stain are purple. HRP-stained fibrils found within protruding and recessed fibripositors are shown in yellow, and unstained fibrils in recessed and protruding fibripositors are green. (*D*) Three-dimensional reconstruction of the stacked serial section tomogram dataset showing a cell membrane (light blue), nucleus (purple), and fibripositor-associated fibrils (yellow) and fibrils in fibricarriers (red). Note: Protruding and recessed fibripositors are not differentiated in the serial tomogram reconstruction because the relatively shallow sample volume (20 μm) precluded their characterization. (Scale bars: *B*, 500 nm; *C*, 2 μm; *D*, 5 μm.)

fibricarriers could occur because they had formed before the 4-h incubation period and remained internal to the cell during the time course of the experiment. Nevertheless, the presence of osmophilic stained fibricarriers is good evidence that they formed at the plasma membrane and pinched off from the membrane during the HRP-incubation period.

Transport of fibricarriers and fibripositors is expected to require a cytoskeletal scaffold and a source of energy. Plasma membrane protrusive structures such as lamellipodia, microspikes, and pseudopodia possess an actin cytoskeleton for scaffolding support. Similarly, fibripositors are actin-dependent protrusions as shown by their disappearance in the presence of cytochalasin B (18). Notably, nocodozole had no affect on fibripositor or fibricarrier structure (18). We showed here using TEM that clouds of fine filaments are present at focal points of contact between the internal membrane of the fibripositor and the luminal collagen fibril. The location of actin filaments in pinch points would explain why cytochalasin B is effective in releasing collagen fibrils from the surface of cells, resulting in the collapse of fibripositors (18).

The formation of fibricarriers at the plasma membrane implies that a pulling force is exerted on the fibril tip. Also, the fact that fibrils in fibripositors are straight is indirect evidence that fibril tips are pulled. In subsequent experiments, we investigated if NMII was responsible for transporting fibricarriers and fibripositors. Blebbistatin was highly effective in inhibiting the contraction of a 3D tendon-like construct. The range in length of the membrane projection of protruding fibripositors (from 1 to 25 μm) suggests a growth process in which membrane is pushed (or pulled) out and retracted. SBF-SEM analyses showed that blebbistatin led to the significant increase in fibripositor mean length (from ∼6 μm to ∼17 μm). Presumably the mean length of the fibripositor is a consequence of NMII-powered inward pulling on the fibripositor and an opposing tissue tension that acts to pull the fibril off the plasma membrane; the pinch points increase stress transfer from the fibril to the plasma membrane and vice versa. The data indicate that NMII is critically involved in the creation and dynamics of fibripositor structures; the exertion of force on fibripositors indicates that these structures are a mechanical interface between the cell and the ECM. Differences were also found in the position of fibrils in protruding and recessed fibripositors: Protruding fibripositor fibrils often project into the matrix, whereas recessed fibripositor fibrils often sit on the plasma membrane. This difference might indicate differences in forces exerted on fibrils in recessed and protruding fibripositors.

Fig. 9 shows a model of a regulatory system that is consistent with data from our laboratory and others. The model shows the following: Initial collagen fibril nucleation can occur at the plasma membrane, fibril formation occurs by accretion of collagen molecules (10, 36) or collagen aggregates (9), subsequent fibripositor formation around individual fibrils is then driven by cellular forces acting on the fibril and depends on the degree of attachment of these fibrils to the cell (via pinch points) and the ECM, and the length of the finger-like portion of the protruding fibripositor is the result of opposing forces of NMII and tissue tension. The finding that fibricarriers can contain fluid-phase HRP and are removed by blebbistatin, dynasore, and DMOG suggests that these fibril-containing compartments can originate at the plasma membrane. Work by others has identified procollagen-containing GPCs en route from the Golgi apparatus to the plasma membrane (8). Therefore, as indicated in Fig. 9, it is possible that fibricarriers could be a type of GPC and might cycle between the plasma membrane and the cytoplasm. Alternatively, fibricarriers might be formed by the inclusion of short early fibrils that are not anchored in the ECM. Consequently, NMII-powered pulling on the fibril would not be counteracted by tissue tension. Importantly, these two schemes are not mutually exclusive, in either case, the short fibril would be encapsulated in a fibricarrier. Internalization of short, nonanchored fibrils to generate fibricarriers may thus be an incidental process in the formation of

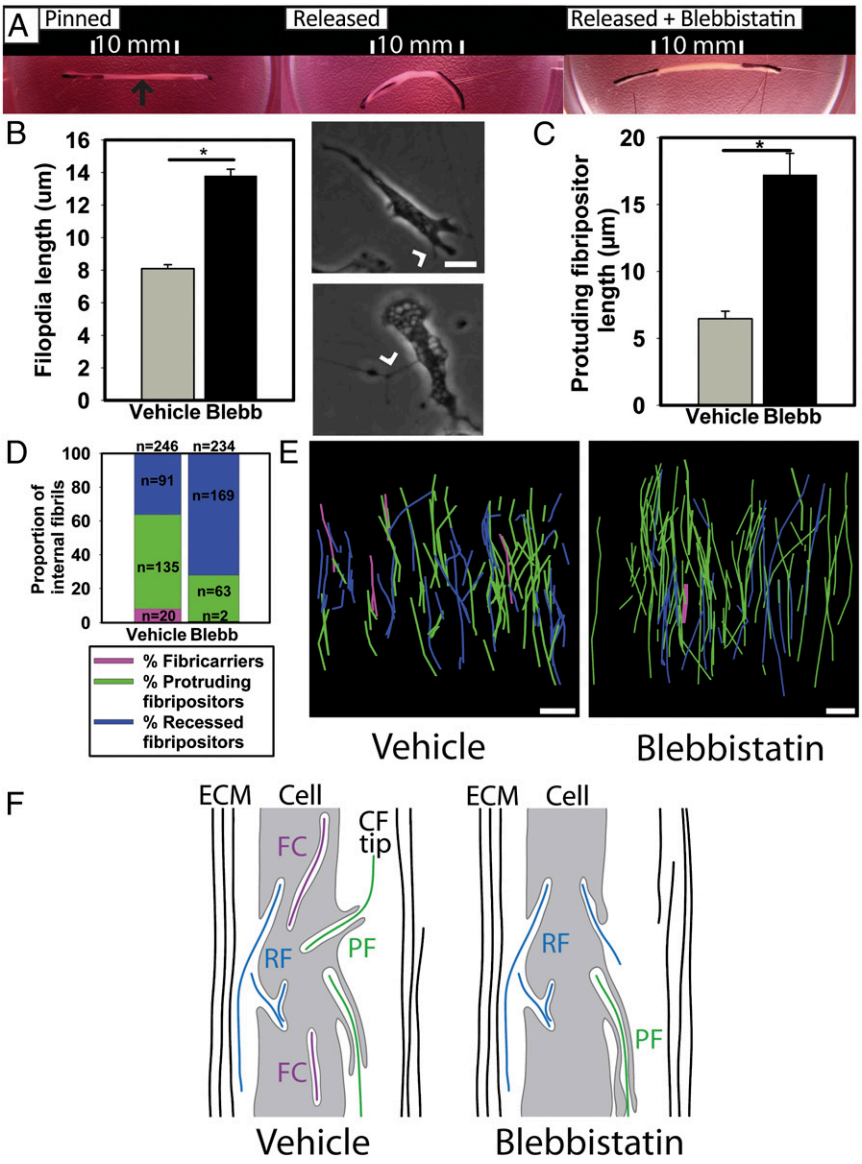

Fig. 6. NMII is required for fibricarrier formation and normal fibripositor membrane dynamics. (*A*) Addition of blebbistatin to tendon-like constructs prevented cell-induced shortening when the constructs were unpinned. Arrow (black) shows the tendon-like construct. (*B*) Protrusive membrane dynamics (such as filopodia formation) are disrupted by blebbistatin. (*Upper Right*) Nonblebbistatin DMSO control. (*Lower Right*) Cell in the presence of blebbistatin. Arrowhead shows filopodia. $*P \leq 0.05$. (*C*) Analysis of 3D EM data showed that the membrane protrusion of protrusive fibripositors is longer when NMII is inhibited in embryonic tendon. Bars show the length of the membrane protrusion ($*P \leq 0.05$). (*D*) The proportion of intracellular fibrils in protrusive fibripositors is decreased when NMII is inhibited with blebbistatin for 4 h. Blebbistatin also reduced the proportion of internal fibrils found in fibricarriers. (*E*) Three-dimensional reconstructions of tendon treated with blebbistatin demonstrate increased numbers of recessed fibripositors (blue) and reduced the numbers of protruding fibripositors (green) with fewer fibricarriers (purple). (*F*) Schematic representation of the effect of NMII inhibition, showing longer fibripositors and fewer fibricarriers. $*P \leq 0.05$. (Scale bars: 5 μm.)

tensioned collagen fibrils. The transport of fibrils from the cell surface into fibricarriers requires membrane scission, as shown when dynasore resulted in the absence of fibricarriers, the deepening of recessed fibripositors, and the concomitant appearance of looped fibrils in deep recesses.

In conclusion, we propose that dynamic transport of new collagen fibrils occurs at the plasma membrane and that this process is driven by NMII. In this scheme, fibripositors are specialized sites of fibril assembly and fibril transport. The fibripositors form an extended mechanical interface between the cytoskeleton and extracellular collagen fibrils. This interface serves to transmit cell-derived tensioning force to the tissue, which is critical in maintaining fibril alignment. In addition, external loads are transmitted back to the cell via fibripositors to provide mechanical feedback during the development of the tissue.

Materials and Methods

Chicken Embryonic Tendon Experiments. Whole chick legs were dissected to expose metatarsal tendons and incubated in DMEM/nutrient mixture F-12 containing 100 units/mL penicillin, 100 μg/mL streptomycin, 2 mM L-glutamine, 200 mM L-ascorbic acid 2-phosphate, supplemented with 25 μM blebbistatin (48 h), 10 μM dynasore (48 h), 1 mM DMOG (48 h), 300 μM leupeptin (48 h), or 0.1% (vol/vol) DMSO. Reagents were purchased from Sigma. Samples were then fixed and processed for EM. The activity of leupeptin to prevent lysosome catheptic enzyme activity was investigated by incubating embryonic chick tendon cells with leupeptin for 2 h, then adding normal media supplemented with leupeptin and fluorescent EGFR (Invitrogen) for 15 min

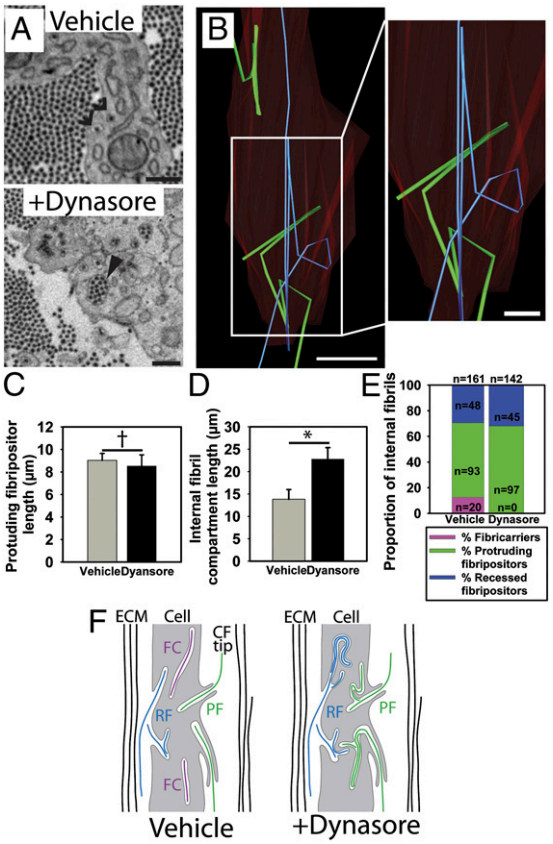

Fig. 7. Inhibition of dynamin reduces the number of fibricarriers. (*A*) SBF-SEM images of embryonic chick tendon treated with dynasore demonstrated the appearance of intracellular fibril compartments containing increased numbers of fibrils (marked with a closed arrowhead). Open arrowheads mark recesses containing single fibrils seen in tendon not treated with dynasore. (*B*) Investigation of this finding in 3D demonstrated that the increased numbers of fibrils seen in 2D cross-sections were the result of internal looping of fibril compartments that were doubled back numerous times. Two different fibrils are shown [in a protruding fibripositor (green) and recessed fibripositor (blue)] illustrating this looping. The cell membrane is colored red. (*C*) There was no difference in the length of the membrane protrusion of protrusive fibripositors. $^{\dagger}P \geq 0.05$. (*D*) Lengths of internal fibril-containing compartments (recessed fibripositors and the internal part of protruding fibripositors) were significantly increased in dynasore-treated tendon cells. $*P \leq 0.05$. (*E*) No fibricarriers were identified in the 142 fibril compartments studied in 3D in dynasore-treated tissue. In contrast, 20 fibricarriers were identified in 161 fibril compartments studied in untreated tissue. (*F*) Schematic showing looped internal fibril recesses and reduced number of fibricarriers after dynasore treatment. (Scale bars: *A*, 500 nm; *B Left*, 5 μm; *B Right*, 2 μm.)

(as described in ref. 37). Cells were washed, incubated in EGFR-free media for a further 30 min, then fixed in 4% (wt/vol) paraformaldehyde and examined by fluorescence microscopy. The inhibition of endocytosis by dynasore was tested by incubation of embryonic chick tendon cells with 25 μg/mL fluorescent transferrin receptor (Tfr488; Invitrogen) for 30 min at 37°C to internalize fluorescent markers. Cells were washed in PBS then incubated with an acid-salt wash buffer (0.2 M HAc and 0.5 M NaCl) for 10 min at 4 °C to strip surface-bound fluorescent marker, followed by PBS wash, and fixed in 4% (wt/vol) paraformaldehyde for 10 min. Internalized fluorescent markers were analyzed by fluorescent light microscopy. Images were collected on an Olympus BX51 upright microscope by using a 60× objective and captured by using a Coolsnap ES camera (Photometrics) through MetaVue Software (Molecular Devices). Specific band-pass filter sets for DAPI, FITC, and Texas red were used to prevent bleed through from one channel to the next.

Serial Block Face-Scanning EM. ***Sample Preparation.*** Samples were prepared as described (20). In brief, metatarsal tendons from embryonic chicks were fixed in situ by using 2% (wt/vol) glutaraldehyde (Agar Scientific) in 0.1 M cacodylate buffer (pH 7.2), *en-bloc* stained in 1% (wt/vol) osmium tetroxide, 1.5% (wt/vol) potassium ferrocyanide in 0.1 M cacodylate buffer, followed by 1% (wt/vol) tannic acid in 0.1 M cacodylate buffer (pH 7.2). After washing, more osmium was added by staining in 1% (wt/vol) osmium tetroxide in 0.1 M cacodylate buffer (pH 7.2). The final staining step involved soaking in 1% (wt/vol) uranyl acetate. Samples were dehydrated in ethanol and infiltrated in Araldite resin (CY212; Agar Scientific).

SBF-SEM. Resin-embedded samples (150 in total during the study) were sectioned by using a Gatan 3View microtome within an FEI Quanta 250 scanning microscope as described (20). For these experiments, a 41 μm × 41 μm field of view was chosen and imaged by using a 4096 × 4096 scan, which gave an approximate pixel size of 10 nm. The section thickness was set to 100 nm in the Z (cutting) direction. Typically, Z volumes datasets comprised 1,000 images (100 μm *z* depth).

Image analysis. The IMOD suite of image analysis software was used to build image stacks, reduce imaging noise, and build 3D reconstructions (23). Fibrils were tracked from their cell-associated tip along the length of the fibril to determine their subcellular localization. Estimates of the length of ECM fibrils were made by tracing individual collagen fibrils (n = 500) over 100 serial images, as described (20). The lengths of fibripositors and fibricarriers were calculated by tracing the complete fibril from its tip in the intracellular recess to its tip in the ECM (n = 50 protruding fibripositors, 50 recessed fibripositors, and 50 fibricarriers from two independent samples). The number of fibripositors (recessed, protruding) and fibricarriers per cell was calculated from IMOD reconstructions of a minimum of four cells for each experimental condition from two independent tendon samples (eight cells in total for DMOG, leupeptin, and DMSO). Each cell was entirely contained within the reconstructed volume. The effect of blebbistatin and dynasore on the length of the membrane protrusion part of protrusive fibripositors was

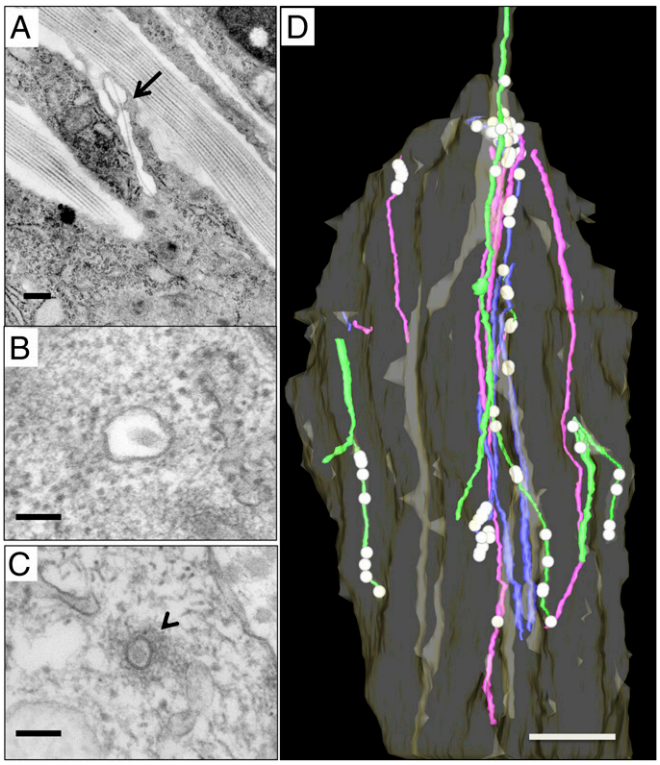

Fig. 8. Pinch points within fibripositors. (*A*) Longitudinal section through an embryonic tendon fibripositor showing a localized constriction of the lumen (arrow). (*B*) Transmission electron micrograph of an interpinch-point lumen (electron lucent) containing a collagen fibril in transverse section. (*C*) Transmission electron micrograph of a "pinch point" in transverse section. The image shows a collagen fibril surrounded by a tightly constricted lumen and a cloud of dense fibrous filaments (arrowhead) in the cytosol. (*D*) Three-dimensional reconstruction of an embryonic tendon cell showing fibrils in protruding fibripositors (green), recessed fibripositors (blue), and fibricarriers (purple). The locations of increased stain density indicative of pinch points are shown as white spheres. (Scale bars: *A*, 500 nm; *B* and *C*, 100 nm; *D*, 2 μm.)

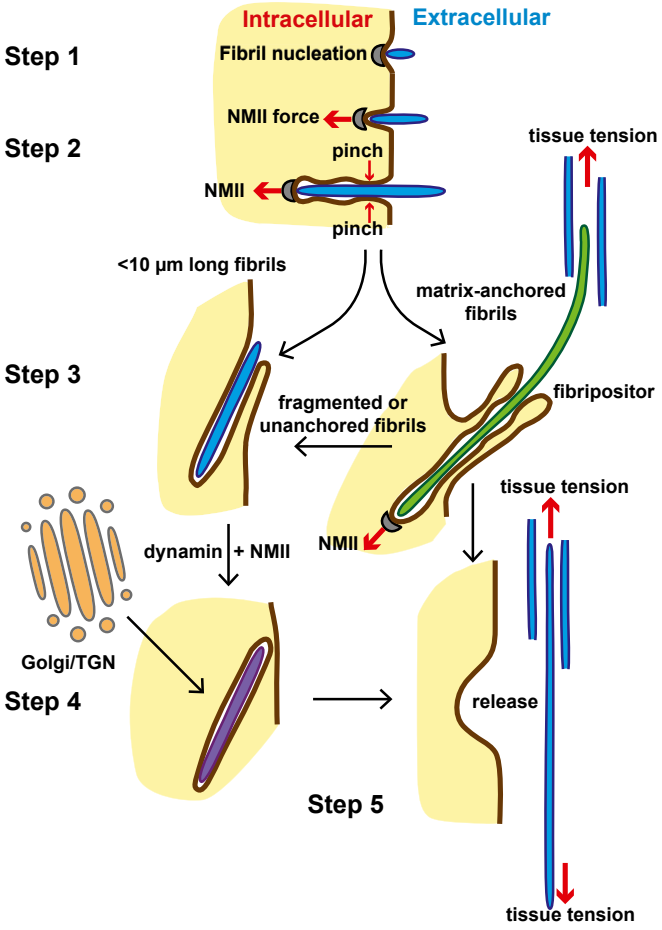

Fig. 9. Model of collagen fibril nucleation and transport. Schematic represents the processes of collagen fibril nucleation and movement between the experimentally-observed compartments. The transportation process is driven primarily by NMII-generated forces. The cell membrane is brown, the cytosol is yellow, and the extracellular matrix is white. Fibrils in protruding fibripositors are green, those in recessed fibripositors are blue, and those in fibricarriers are purple. Collagen fibrils are formed at the cell surface by nucleation of collagen (step 1). Newly formed fibrils are pulled into a membrane recess by NMII (step 2). Fibrils continue to grow by molecular accretion, and tension is continually exerted on these fibrils by NMII. Long fibrils contained in protruding fibripositors are positioned in the matrix, whereas short fibrils remain in recessed fibripositors (step 3). Fragmented or unanchored fibrils may be totally internalized in a process requiring NMII and dynamin, forming fibricarriers. Fibrils inside fibricarriers may grow by secretion of collagen from the Golgi/TGN apparatus (step 4). Fibricarriers secrete their fibril cargo back into the ECM (step 5). We propose that the tension exerted on matrix-anchored fibrils in fibripositors by NMII-generated cell force is important in generating an aligned tissue that is tensioned.

calculated from 3D reconstructions (n = 50 measured for control and blebbistatin-treated tendon). In blebbistatin experiments, the proportion of fibrils found in fibripositors and fibricarriers was summed for two independent samples (two DMSO and two blebbistatin). The number of fibrils analyzed was 246 (DMSO control) and 234 (blebbistatin-treated samples). To confirm action of MMP inhibitors, aliquots of medium conditioned by embryonic chick tendon cells were analyzed by gelatin zymography in 0.1% gelatin-10% acrylamide gels (38). Aliquots of appropriately diluted media were loaded without reduction on gels at 10 μL. After electrophoresis, gels were washed with 2.5% Triton X-100 to remove SDS and renature the MMP-2 species in the gels. Then the gels were incubated in the developing buffer overnight to induce gelatin lysis by renatured MMP-2. MMP-2 standards were obtained from ProteaImmun.

Immunoelectron Microscopy. Samples for immunolabeling were fixed in 4% formaldehyde in 0.1 M phosphate buffer (pH 7.2), embedded in 12% gelatin (wt/vol), and infiltrated with 20% polyvinylpyrrolidon (wt/vol) and 1.6 M sucrose. The samples were frozen in liquid nitrogen, and ultrathin 70-nm sections were cut at −120 °C with a Leica UC6/FC6 cryoultramicrotome. Sections were retrieved with methylcellulose/sucrose (1%/1.15 M) and put on carbon/formvar-coated nickel grids. The sections were blocked with 1% (wt/vol) BSA and 0.15 M glycine in 0.1 M phosphate buffer (pH 7.2), and labeled with primary antibodies against LAMP2 (ABR, PA1-655, dilution 1:10) and protein A gold conjugates (10 nm). The grids were embedded in 1.8% (wt/vol) methylcellulose with 0.5% (wt/vol) uranyl acetate and examined in a Tecnai 12 BioTwin electron microscope.

HRP Tracer Experiment and Electron Tomography. Embryonic chick metatarsal tendon was incubated in culture medium containing L-ascorbic acid supplemented with 1 mg/mL HRP (Sigma) for 4 h. Tissue was fixed in 2% glutaraldehyde, DAB-hydrogen peroxide solution was added for 30 min at 4°C in a light-free environment, and then prepared for TEM by using a standard *en-bloc* osmium and uranyl acetate stain. Samples were prepared for electron microscopy and serial section reconstruction as described (17). Semithick (300 nm) serial sections were collected on formvar-coated copper slot grids. The serial sections were imaged in an FEI Polara 300 kV transmission electron microscope by using SerialEM (39). Within SerialEM, a macro was written to move to a specified grid position, find the eucentric height, then collect single-axis tomograms (±60° every 2°, 4k × 4k binning 1) at low magnification (~5 nm pixel size) to generate a tomogram for each section on the grid. Tomograms were generated in IMOD by using the patch-tracking algorithm (23). Each tomogram was compressed in Z by a factor of 6 to reduce the total file size, which gave the final reconstruction an approximate voxel size of 5 nm × 5 nm × 30 nm, which is comparable to standard serial section reconstructions. The tomograms were crudely aligned by using tools in the IMOD suite, and the volume was examined and modeled by using IMOD. For some images, the models were exported as VRML files and imported into Amira, where they were realigned to a binned dataset.

Pulse–Chase Analysis of Procollagen Processing and Secretion. Embryonic chick metatarsal tendon (preincubated with 1 mM DMOG or 0.1% DMSO for 1 h) was subjected to [^{14}C]-proline labeling as described (18, 40). Reagents were obtained from Invitrogen or Sigma unless stated otherwise. Pulse–chase experiments were performed at 37 °C in DMEM/nutrient mixture F-12 containing 100 units/mL penicillin, 100 μg/mL streptomycin, 2 mM L-glutamine, 200 mM L-ascorbic acid 2-phosphate, and 400 mM β-aminopropionitrile. Pulse–chase experiments were performed at 37 °C; tendons were preequilibrated for 30 min, labeled for 10 min with 2.5 μCi/mL [^{14}C]-proline (GE Healthcare), and then transferred to unlabeled medium for 15 min to 3 h. Pulse–chase was stopped by transferring the tendons to 25 mM EDTA and 50 mM Tris·HCl (pH 7.5) at 4 °C. Tendons subjected to pulse–chase analysis in 100-μL aliquots of supplemented medium were then extracted in 100-μL aliquots of salt extraction buffer (1 M NaCl, 25 mM EDTA, and 50 mM Tris·HCl at pH 7.5) containing protease inhibitors and supplemented as required with Nonidet P-40 detergent (1%, vol/vol). A concentrated stock solution of protease inhibitors was made by using EDTA-free protease inhibitor mixture tablets (Roche Applied Science). Tendons were extracted in four changes of salt extraction buffer [overnight (S1), 6 h (S2), overnight (S3), and 6 h (S4)] and overnight in salt extraction buffer containing Nonidet P-40. Extracts were analyzed by using 4% precast SDS-polyacrylamide gels (Novex) under reducing conditions. The gels were fixed for 40 min by using two changes of methanol (10%, vol/vol) and acetic acid (10%, vol/vol) and dried under vacuum. The gels were exposed to a BAS-MS phosphorimaging plate (Fujifilm), which was processed by using an FLA3000 phosphoimager (Fujifilm). Protein extracts were examined by standard Western blot procedures and optimal antibody dilutions determined empirically. Anti–β-actin antibodies were obtained from Sigma (mouse monoclonal AC-15 A5441).

Tendon-Construct Formation. Tendon constructs were assembled as described (33, 34). Constructs were incubated with 25 μM blebbistatin for 30 min before release. Contraction of tendon constructs was observed over ~15 min.

Live-Cell Imaging of Tendon Cells. Embryonic tendon cells were treated with either 0.1% DMSO, or 25 μM blebbistatin and imaged by using an AS MDW live-cell imaging system (Leica) with a 20×/0.5 HC Plan Fluotar objective. Point visiting was used to allow multiple positions to be imaged within the same time-course, and cells were maintained at 37 °C and 5% CO_2. Cells were incubated for 1 h before imaging. Images were collected every 10 s for 10 min by using a Cascade II EM CCD camera for ultrasensitive imaging (Photometrics). The still images were converted into a movie file by using ImageJ (NIH freeware; http://rsb.info.nih.gov/nih-image). Three samples treated with

blebbistatin, and three treated with DMSO were analyzed. Maximum filopodia length was measured by using ImageJ (100 measurements per sample).

Statistical Analysis. Statistical analyses were performed by using SPSS version 14. Differences in fibripositor and filopodia length and number of fibripositors and fibricarriers per cell were examined by using Student's *t* test. Significance was set at $P < 0.05$. Data are presented as mean ± SEM.

ACKNOWLEDGMENTS. We thank the Wellcome Trust for generous support by Grants 091840/Z/10/Z, 083898/Z/07/Z, and 081406/Z/06/Z.

1. Mironov AA, et al. (2003) ER-to-Golgi carriers arise through direct en bloc protrusion and multistage maturation of specialized ER exit domains. *Dev Cell* 5(4):583–594.
2. Leblond CP (1989) Synthesis and secretion of collagen by cells of connective tissue, bone, and dentin. *Anat Rec* 224(2):123–138.
3. Saito K, et al. (2009) TANGO1 facilitates cargo loading at endoplasmic reticulum exit sites. *Cell* 136(5):891–902.
4. Venditti R, et al. (2012) Sedlin controls the ER export of procollagen by regulating the Sar1 cycle. *Science* 337(6102):1668–1672.
5. Stephens DJ (2012) Cell biology: Collagen secretion explained. *Nature* 482(7386): 474–475.
6. Trucco A, et al. (2004) Secretory traffic triggers the formation of tubular continuities across Golgi sub-compartments. *Nat Cell Biol* 6(11):1071–1081.
7. Bonfanti L, et al. (1998) Procollagen traverses the Golgi stack without leaving the lumen of cisternae: Evidence for cisternal maturation. *Cell* 95(7):993–1003.
8. Polishchuk RS, et al. (2000) Correlative light-electron microscopy reveals the tubular-saccular ultrastructure of carriers operating between Golgi apparatus and plasma membrane. *J Cell Biol* 148(1):45–58.
9. Bruns RR, Hulmes DJ, Therrien SF, Gross J (1979) Procollagen segment-long-spacing crystallites: Their role in collagen fibrillogenesis. *Proc Natl Acad Sci USA* 76(1): 313–317.
10. Kadler KE, Holmes DF, Trotter JA, Chapman JA (1996) Collagen fibril formation. *Biochem J* 316(Pt 1):1–11.
11. Canty-Laird EG, Lu Y, Kadler KE (2012) Stepwise proteolytic activation of type I procollagen to collagen within the secretory pathway of tendon fibroblasts in situ. *Biochem J* 441(2):707–717.
12. Canty EG, Kadler KE (2005) Procollagen trafficking, processing and fibrillogenesis. *J Cell Sci* 118(Pt 7):1341–1353.
13. Bruckner P (2010) Suprastructures of extracellular matrices: Paradigms of functions controlled by aggregates rather than molecules. *Cell Tissue Res* 339(1):7–18.
14. Chapman JA (1989) The regulation of size and form in the assembly of collagen fibrils in vivo. *Biopolymers* 28(8):1367–1382.
15. Trelstad RL, Hayashi K (1979) Tendon collagen fibrillogenesis: Intracellular subassemblies and cell surface changes associated with fibril growth. *Dev Biol* 71(2): 228–242.
16. Birk DE, Trelstad RL (1986) Extracellular compartments in tendon morphogenesis: Collagen fibril, bundle, and macroaggregate formation. *J Cell Biol* 103(1):231–240.
17. Canty EG, et al. (2004) Coalignment of plasma membrane channels and protrusions (fibripositors) specifies the parallelism of tendon. *J Cell Biol* 165(4):553–563.
18. Canty EG, et al. (2006) Actin filaments are required for fibripositor-mediated collagen fibril alignment in tendon. *J Biol Chem* 281(50):38592–38598.
19. Leighton SB (1981) SEM images of block faces, cut by a miniature microtome within the SEM - a technical note. *Scan Electron Microsc* (Pt 2):73–76.
20. Starborg T, et al. (2013) Using transmission electron microscopy and 3View to determine collagen fibril size and three-dimensional organization. *Nat Protoc* 8(7): 1433–1448.
21. Jaakkola P, et al. (2001) Targeting of HIF-alpha to the von Hippel-Lindau ubiquitylation complex by O2-regulated prolyl hydroxylation. *Science* 292(5516):468–472.
22. Macia E, et al. (2006) Dynasore, a cell-permeable inhibitor of dynamin. *Dev Cell* 10(6): 839–850.
23. Kremer JR, Mastronarde DN, McIntosh JR (1996) Computer visualization of three-dimensional image data using IMOD. *J Struct Biol* 116(1):71–76.
24. Beertsen W, Brekelmans M, Everts V (1978) The site of collagen resorption in the periodontal ligament of the rodent molar. *Anat Rec* 192(2):305–317.
25. Melcher AH, Chan J (1981) Phagocytosis and digestion of collagen by gingival fibroblasts in vivo: A study of serial sections. *J Ultrastruct Res* 77(1):1–36.
26. Garant PR (1976) Collagen resorption by fibroblasts. A theory of fibroblastic maintenance of the periodontal ligament. *J Periodontol* 47(7):380–390.
27. Rifkin BR, Heijl L (1979) The occurrence of mononuclear cells at sites of osteoclastic bone resorption in experimental periodontitis. *J Periodontol* 50(12):636–640.
28. Everts V, Beertsen W (1987) The role of microtubules in the phagocytosis of collagen by fibroblasts. *Coll Relat Res* 7(1):1–15.
29. Everts V, Beertsen W, Schröder R (1988) Effects of the proteinase inhibitors leupeptin and E-64 on osteoclastic bone resorption. *Calcif Tissue Int* 43(3):172–178.
30. Cuervo AM, Dice JF (1996) A receptor for the selective uptake and degradation of proteins by lysosomes. *Science* 273(5274):501–503.
31. Tabata K, et al. (2010) Rubicon and PLEKHM1 negatively regulate the endocytic/autophagic pathway via a novel Rab7-binding domain. *Mol Biol Cell* 21(23):4162–4172.
32. Meshel AS, Wei Q, Adelstein RS, Sheetz MP (2005) Basic mechanism of three-dimensional collagen fibre transport by fibroblasts. *Nat Cell Biol* 7(2):157–164.
33. Kapacee Z, et al. (2008) Tension is required for fibripositor formation. *Matrix Biol* 27(4):371–375.
34. Kalson NS, et al. (2010) An experimental model for studying the biomechanics of embryonic tendon: Evidence that the development of mechanical properties depends on the actinomyosin machinery. *Matrix Biol* 29(8):678–689.
35. Rösner H, Möller W, Wassermann T, Mihatsch J, Blum M (2007) Attenuation of actinomyosinII contractile activity in growth cones accelerates filopodia-guided and microtubule-based neurite elongation. *Brain Res* 1176:1–10.
36. Trotter JA, Kadler KE, Holmes DF (2000) Echinoderm collagen fibrils grow by surface-nucleation-and-propagation from both centers and ends. *J Mol Biol* 300(3):531–540.
37. Everts V, Beertsen W, Tigchelaar-Gutter W (1985) The digestion of phagocytosed collagen is inhibited by the proteinase inhibitors leupeptin and E-64. *Coll Relat Res* 5(4):315–336.
38. Deryugina EI, et al. (2001) MT1-MMP initiates activation of pro-MMP-2 and integrin alphavbeta3 promotes maturation of MMP-2 in breast carcinoma cells. *Exp Cell Res* 263(2):209–223.
39. Mastronarde DN (2005) Automated electron microscope tomography using robust prediction of specimen movements. *J Struct Biol* 152(1):36–51.
40. Humphries SM, Lu Y, Canty EG, Kadler KE (2008) Active negative control of collagen fibrillogenesis in vivo. Intracellular cleavage of the type I procollagen propeptides in tendon fibroblasts without intracellular fibrils. *J Biol Chem* 283(18):12129–12135.